DOI 10.1007/s11182-024-03269-z

Russian Physics Journal, Vol. 67, No. 9, September, 2024

STRUCTURE AND PROPERTIES OF A WELDED JOINT OF A CORROSION-RESISTANT NICKEL ALLOY USED FOR WORK IN MOLTEN SALTS

P. K. Chuquimarca, D. V. Pyrin, K. O. Ivanov, K. S. Eltysheva, A. Yu. Zhilyakov, and S. V. Belikov

UDC 539.5

In this paper, an isothermal diagram of the second phase formation in the Hastelloy G35 alloy was constructed to understand possible phase transformations during welding. A welded joint has been studied in three areas: fusion zone (FZ), the heat affected zone (HAZ), and the base metal (BM). The FZ is represented by a dendritic structure; in addition, σ-phase intermetallic compounds are present in the FZ and HAZ. Furthermore, the FZ and BM present similar hardness values, while the hardness increases in the HAZ. It has been established that thermal effects for different areas are characterized by different rates of increase up to 650°C.

Keywords: Ni–Cr–Mo alloy, corrosion-resistant alloy, isothermal diagram, welded joint, hardness, differential thermal analysis, specific heat capacity.

INTRODUCTION

Many industries, especially chemical engineering, are based on continuous development and improvement of materials with high properties and their ability to resist harsh environments. This is one of the main reasons for continued research on commercial Ni-based alloys, since they concern almost all industries the products of which must withstand not only high temperatures, but also extremely aggressive environment, especially corrosive one [1].

The Hastelloy® G-35® alloy belongs to the group of corrosion-resistant alloys based on the Ni–Cr–Mo system. It was developed by Haynes International, Inc. at the beginning of the first decade of the XXI century and is characterized by high corrosion resistance during *wet processes* with phosphoric acid, oxidizing acids, and chloride-bearing media; in addition, it is designed to resist localized attacks when working with chlorides, thereby conferring a good resistance to chloride-induced stress corrosion cracking [2–3]. In addition, the Hastelloy® G-35® alloy has found relevance in oxidative leaching technology field and metal etching [2]; it is also promising as a structural material for the safe storage of nuclear waste [4]. As well as other alloys based on the Ni–Cr–Mo system, this material is considered to be a candidate for use in contact with aggressive salt and metal melts [4–6].

In the current research, the focus on welding of the Hastelloy® G-35® alloy mainly relies on the evaluation of the influence of welding procedure on microstructural changes, hardness, and specific heat capacity from welded joints. During exploitation, the material experiences long periods of time exposed to high temperatures and molten salts. Previous studies have shown a corrosion resistance for 100 h. In work [7], the material corrosion resistance was studied with particular emphasis on the development of local corrosion, intergranular corrosion, and microstructural morphology changes. Several investigations were focused on the structural changes of the Hastelloy® G-35® alloy exposed to molten salts [4–7]. The σ-phases and carbides were registered after exposure to high temperatures and were classified as an undesirable phase that negatively affects the corrosion resistance [8]. However, these investigations

Ural Federal University, Yekaterinburg, Russia, e-mail: f.pomagualli@gmail.com, d.v.pyrin@gmail.com, konstantin.ivanov@urfu.ru, kristina.eltysheva@urfu.ru, a.y.zhilyakov@urfu.ru, s.v.belikov@urfu.ru. Original article submitted July 18, 2024, accepted for publication August 22, 2024.

were focused on the Hastelloy® G-35® alloy in the as-received state and paid little attention to welding processes. Moreover, it is well known that different structures (dendrites, partial recrystallized grains, carbides, etc.), which can get formed along the joint after the welding procedures, can affect the physical and mechanical properties of the material. When creating structures from such alloys, one of the problems is the localization of corrosion damage near welded joints or inside welds. Therefore, the question of the structure and phase formation during welding of nickel–chromium–molybdenum alloys becomes important.

EXPERIMENTAL

The MIG welding procedure was carried out with the following parameters: the single pass weld with a current of 150 A, speed of 160 mm/min, and gas (Ar) flow rate of 10 l/min. The selected welding filler material was ENiCrMo-22 (Table 1) chosen by its chemical compatibility with the base material. The tests were carried out for the welded joint of a nickel-based Hastelloy G-35 pipe with a thickness of 4 mm and diameter of 89 mm. The as-received state consisted of a single hot rolling operation.

Metallographic analysis was performed using a Jeol JSM-6490 LV scanning electron microscope with an Inka Energy TEM 350 microanalysis attachment. Samples were prepared according to the ASTM E47/ E3 standards using a cutting procedure followed by grinding on a sandpaper board in a sequential abrasive fraction reduction using the Struers LaboPol-5 system to finally polish the samples on a decrease diamond particles suspension (9–1 μm) plus colloidal silicon suspension. Any contamination during sample preparation, a gentle air flow was used to remove dust particles or distilled water. Since the area of interest is a welded seam, microscopy was performed along the three characteristic zones that a weld bead is commonly divided: fusion zone (FZ), heated affected zone (HAZ), and material base (MB).

The hardness tests were performed on a micro-hardness tester (CSM Instruments), while the values were determined by the Oliver and Pharr method. Samples consisted of cut parts of the welded joint, and measurements were performed at a load of 9 N with a pause of 15 s during indentation at a loading/unloading speed of 18 N/min. The test procedure was carried out at room temperature along the welded joint.

The specific heat capacity measurement (of the DSC curves) was carried out using the NETZSCH STA 449 C F3 Jupiter thermal analyzer in the following testing conditions: an argon atmosphere with a gas flow rate of 20 ml/min and heating rate of 20 K/min in the temperature range 30…800°C. As part of the process of differential scanning calorimetry (DSC) evaluation, samples were prepared from each characteristic zones of the welded seam, including the fusion zone, heat affected zone, and base material. The sample dimensions were as follows: a diameter of 5 mm and a thickness of 1 mm. A total of 4 samples, 2 from HAZ and 2 from FZ zones, were cut from the BM.

RESULTS

Since the areas adjacent to the resulting melt are affected by the heating bath during the welding process due to the temperature gradient between the melt bath and the base metal, a C-shaped temperature-time-transformation diagram of the release of excess phases during isothermal exposure was constructed for the G-35 alloy to predict possible phase transformations (Fig. 1).

Metallographic analysis of the microstructure of the samples after various exposure times and temperatures was carried out. The closed circles in the diagram indicate the presence of secondary phases under these conditions, while the open circles indicate their absence. The solid curve here corresponds to the beginning of the formation of the second phases. It was found that at temperatures around 800–900°C, the processes of separation of intermetallic compounds along grain boundaries begin after a fifteen-minute exposure.

Figure 2 shows the macrostructure of the welded joint. This study did not detect defects such as pores, hot cracks, undercuts, non-welding, etc., which confirms a high-quality weld. The red straight lines indicate the trajectories of hardness measurement. The microstructure was studied in the three areas that characterize the welded joint: FZ, HAZ, and BM (Fig. 3). The FZ is characterized by the dendritic structure oriented mainly along the heat dissipation

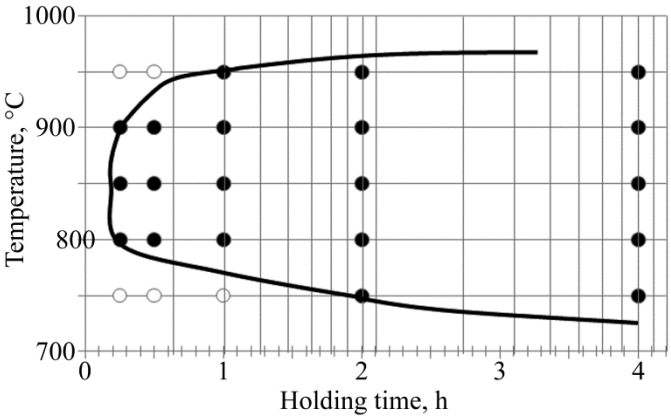

Fig. 1. Isothermal diagram of the separation of secondary phases in the G-35 alloy after isothermal exposure.

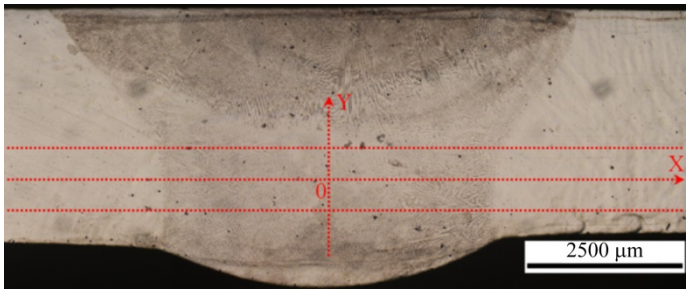

Fig. 2. Macrostructure of the G-35 alloy welded joint.

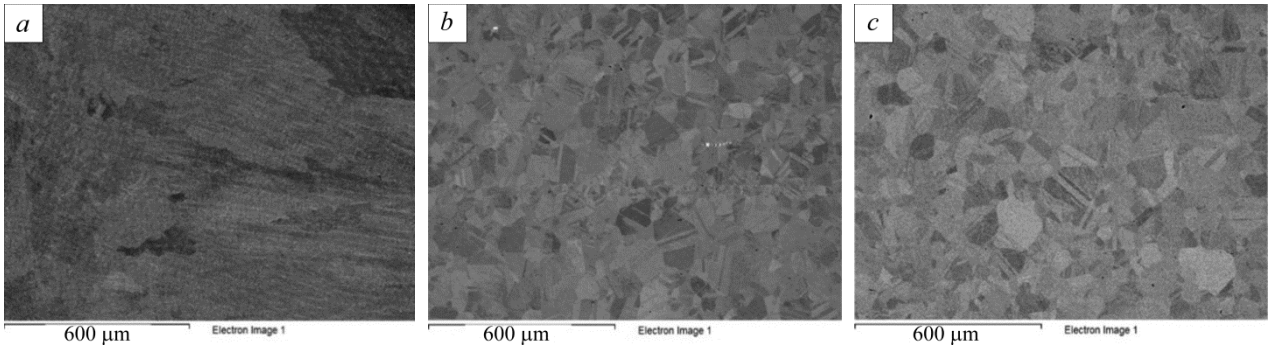

Fig. 3. Areas of the microstructure characteristic of the welded joint: FZ (*a*), HAZ (*b*), and BM (*c*).

direction. The equiaxed grains are observed in the HAZ and BM. At high magnifications, the microstructure in the FZ and HAZ (Fig. 4) showed the presence of rounded particles of secondary phase (as expected when constructing the isothermal diagram).

Table 1 presents the G-35 chemical composition according to the UNS N060355/ASTM B619 standards with the ENiCrMo-22 filler and the results of the EDS analysis of the BM and FZ.

As follows from Table 1, the chemical composition of the alloy satisfies to the requirements of the standards as well as demonstrates that it does not change during the welding process due to possible burnout of the elements under

TABLE 1. Chemical Composition of the Hastelloy G-35 and ENiCrMo-22 filler according to the ASTM B619 and AWS A5.11 Standards and the Results of EDS Analysis of the FZ and BM

As demanded by the standard or delivery	Content of the elements, wt.%							
	Ni	Cr	Mo	Fe	Si	Mn	Al	C
Standardized by UNS N06035, ASTM B619	BAL	33	8	2*	0.6*	0.5*	0.4*	0.05*
Standardized by UNS W86022, AWS A5.11	BAL	32–34	7.6–9	2*	0.6*	0.5*	0.4*	0.05*
BM	56.7	34.5	7.5	1.3	–	–	–	–
FZ	57.8	33.5	7.4	1.3	–	–	–	–

Note: Here * indicates the maximum value.

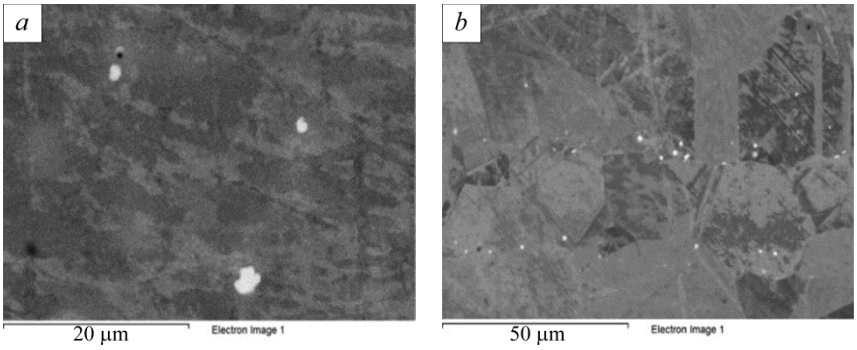

Fig. 4. Microstructure of the FZ (*a*) and HAZ (*b*) at high magnifications demonstrating the presence of the second phase particles.

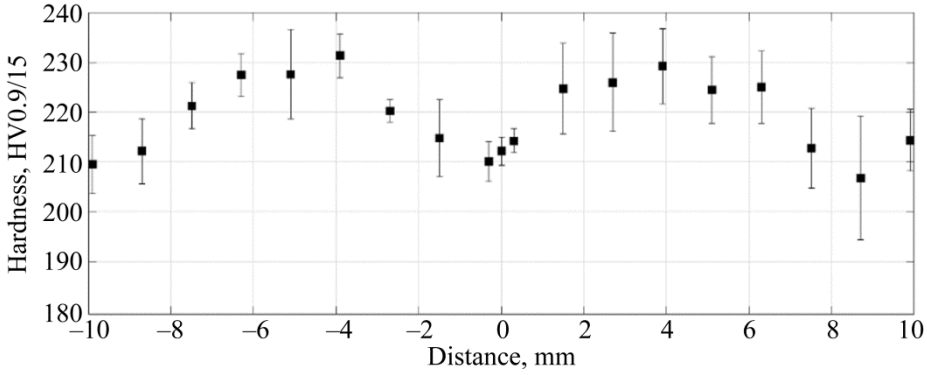

Fig. 5. Hardness Vickers test graphic results from the G 35 welded pipe sample.

the influence of the local high temperature condition. From the results of hardness tests of the welded joint samples (Fig. 5), it can also be seen that the HAZ is characterized by high hardness values, and similar values are observed for the FZ and BM.

The onset and end phase transformation temperatures were determined through the evaluation of the exothermal and endothermal effects in the DSC curves. Figure 6 shows the change in the heat capacity of the alloy samples taken from the characteristic zones of the welded joint. The effect (marked with the dashed straight lines) is observed in the temperature range of 250–500°C. The decrease in the curve before reaching the first inflection point at 400°C is more pronounced for the base metal samples. After that, there is a local decrease in the heat capacity as the temperature increases, followed by its increase. The beginning of this effect for the samples is marked with the arrows.

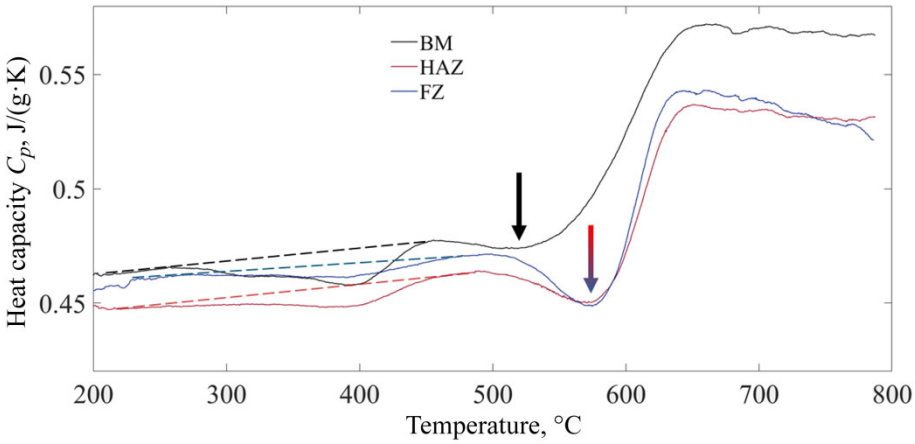

Fig. 6. Heat capacity versus temperature diagram for the G35 alloy.

For the BM samples, the transformation begins at a lower temperature (510°C), while the initial temperatures for the HAZ and FZ samples are higher, 571 and 574°C, respectively. Despite the temperature difference at the beginning of the transformation, the effect stops in the samples taken from different regions at a temperature of approximately 650°C.

DISCUSSION

Figure 1 shows that during the short-term heating of the alloy in the temperature range of 800–900°C, the processes of excess release of undesirable phases begin. Hence, it is expected that the particles of the second phases will be detected, which can negatively affect the corrosion resistance of the material because of the depletion of grain boundaries in Cr and Mo. These results are confirmed by the fact that the excess phases were detected in the FZ and HAZ of the welded joint (Fig. 4). The base metal was characterized by the presence of prior austenite coarse grains without secondary phases or carbides. There were almost no changes in the HAZ compared to the base metal; the matrix was formed by similar austenitic grains. However, at high magnification, the presence of small bright particles was registered. In previous work [9] devoted to the study of the characteristics of the Hastelloy alloy, these bright particles were defined as the σ-phase. A strong presence of these small particles was recorded in the thermally affected zone located close to the austenitic grain boundaries. This was the area with the greatest amount of the registered σ-phase, especially in the HAZ center.

The morphology of the welded well appears to follow the heat input direction during cooling of the weld bead having a dendritic columnar structure. Such microstructure formation is the product of differences between the temperature and composition during solidification [10]. The dendrites are oriented approximately parallel to the surface of the all-weld metal cross section; similar dendritic growth was described by H. Schönmaier *et al*. [11]. In addition, it was found that the scattered σ-phase particles found in the weld are characterized by large sizes compared with the particles from the HAZ.

The hardness distribution along the center of the welded joint cross section exhibits symmetrical values (the indentation positions are shown in Fig. 2). The presence of the maximum hardness (around 230 HV) was registered in the HAZ; when moving toward the FZ, it can be observed that the hardness values drop and reach the value around 210 HV. Similar behavior can be observed when moving toward the BM where the hardness decreased approximately to 209 HV. Hence, the BM had the lowest hardness in the whole joint. In this case, the hardness is related to dislocation density and residual stress; this last one is the product of the thermal, microstructural, and thermo-elastoplastic changes generated by the localized application of heat to melt the material and form the joint. When the material solidifies, the stresses are created around the weld area, due to which the HAZ has a higher hardness.

In work [12] it was shown that the formation of the ordered $Ni_2(Cr, Mo)$ phase is possible in the alloys of the Ni–Cr–Mo system; hence, the low-temperature effects of the material under study in the range of 250–450°C are associated with this phase. In the case of the base metal, where the chemical elements are more uniformly distributed, the generation of a larger number of particles of the $Ni_2(Cr, Mo)$ phase is possible; as a result, the effect (the deviation of the black curve from the dashed straight line) is more pronounced. In the case of the chemically inhomogeneous material in the fusion zone, due to the enrichment in Cr and Mo of interdendritic spaces, the effect is less due to smaller areas of possible formation of this phase. A further decrease in the heat capacity curves is associated with the increase of the formed particles more pronounced in the fusion zone. After the inflection points denoted by the arrows, the previously formed particles of the $Ni_2(Cr, Mo)$ phase dissolve. Again, the effect is shifted toward higher temperatures in the fusion and heat-treated zones. In addition, the less pronounced growth of the base metal curve is observed. However, despite the beginning temperature, the dissolution ends at approximately the same temperatures of about 650°C.

CONCLUSIONS

1. The C-shaped diagram of the secondary phase formation in the G35 alloy after isothermal exposure from 750 to 950°C has been constructed. It was found that the formation of particles occurs already after a fifteen-minute exposure at a temperature of 850°C.

2. It was shown that no defects characteristic of the welding process were found in the sample of the welded joint. The high heat input by welding affects the formation of different structures in the welded joint. The microstructure of the fusion zone is characterized by the columnar dendritic structure. The heat affected zone and the base metal are represented by the austenitic grains. It was found that the release of the σ-phase particles was present in the fusion zone (in the interendritic space) and heat affected zone (along the grain boundaries).

3. The hardness profile of the welded joint had increased values (231 ± 4 HV) characteristic of the heat affected zone, which is associated with the high stress level in this area. The base metal and fusion zones had similar hardness values of 207 ± 2 HV and 210 ± 7 HV, respectively.

4. It was found that the formation and dissolution of particles of the ordered $Ni_2(Cr, Mo)$ phase in the fusion zone was shifted toward higher temperatures. The different magnitudes of the effects were due to different chemical uniformity degrees of the metal in different zones of the welded joint. Regardless of the temperature at which the formation/dissolution of this phase began, the effect ended at approximately the same temperature in different areas of the welded joint.

COMPLIANCE WITH ETHICAL STANDARDS

Author contributions

P.D.V., C.P.K., and Zh.A.Yu. were involved in planning and supervised the work; C.P.K., E.K.S., I.K.O., and P.D.V. prepared the samples and characterized them with the JEOL JSM-6490 LV scanning electron microscope; C.P.K. and P.D.V. carried out the determination of the specific heat capacity and hardness characterization; C.P.K., I.K.O., and P.D.V. processed the experimental data, performed the analysis, drafted the manuscript, and designed the figures; P.D.V., C.P.K., Zh.A.Yu., and B.S.V. contributed to the interpretation of the results and worked on the manuscript. All authors discussed the results and commented on the manuscript. All authors have read and agreed to the published version of the manuscript.

Conflicts of interest

The authors declare that they have no known competing financial interests or personal relationships that could have appeared to influence the work reported in this paper.

Funding

The work was supported by the Ministry of Science and Higher Education of the Russian Federation within the framework of the Development of the Strategic Academic Leadership Program "Priority 2030" of Ural Federal University named after the First President of Russia B. N. Yeltsin.

Financial interests

The authors declare they have no relevant financial or non-financial interests to disclose.

Institutional review board statement

Applicable.

REFERENCES

1. A. Ramu, V. Pavlik, V. Sillikova, O. Matselko, and M. Boca, Mater. Corros., **74** (5), 670–682 (2023); https://doi.org/10.1002/maco.202213412.
2. G. M. Chirieleison, G. L. Hoback, P. Crook, *et al*., Weld. J., **87**, No. 5, 119–123 (2008).
3. P. Houlle and M. Chagraoui, Procedia Eng., **46**, 279–284 (2012); DOI: 10.1016/j.proeng.2012.09.473.
4. N. Keskar, A. K. Pattanaik, K. V. Mani Krishna, *et al*., Metall. Mater. Trans. A, **48**, 3096–3107 (2017); https://doi.org/10.1007/s11661-017-4066-1.
5. K. C. Tekin and U. Malayoglu, Tribol. Lett., **37** (3), 563–572 (2010); DOI: 10.1007/s11249-009-9552-1.
6. A. Laureys, E. Wallaert, L. Claeys, *et al*., Procedia Struct. Integr., **42**, 1458–1466 (2022); https://doi.org/10.1016/j.prostr.2022.12.186.
7. A. Ramu, V. Pavlik, V. Sillikova, and M. Boca, Materials, **16**, 2679 (2023); https://doi.org/10.3390/ma16072679.
8. J.-O. Nilsson, P. Kangas, A. Wilson, and T. Karlsson, Metall. Mater. Trans. A, **31**, 35–45 (2000); DOI: 10.1007/s11661-000-0050-1.
9. H. M. Tawancy, J. Mater. Sci., **18**, 2976–2986 (1983); https://doi.org/10.1007/BF00700780.
10. S. A. David and J. M. Vitek, Int. Mater. Rev., **34** (5), 213–245 (1989); DOI: 10.1179/imr.1989.34.1.213.
11. H. Schönmaier, R. Krein, M. Schmitz-Niederau, and R. Schnitzer, J. Mater. Eng. Perform., **30** (10), 7138–7151 (2021); DOI: 10.1007/s11665-021-05922-x.
12. The SAO Astrophysics Data System; https://ui.adsabs.harvard.edu/abs/2021JMEP...30.7138S/abstract.
13. A. Y. Zhilyakov, S. V. Belikov, A. F. Gibadullina, *et al*., Met. Sci. Heat Treat., **11–12**, 792–797 (2020); https://doi.org/10.1007/s11041-020-00502-7.